materials

MDPI

Article

Electrochemical Performances Investigation of New Carbon-Coated Nickel Sulfides as Electrode Material for Supercapacitors

Xinyu Lei, Mu Li, Min Lu and Xiaohui Guan *

School of Chemical Engineering, Northeast Electric Power University, Jilin 132000, China; leixinyu_k@163.com (X.L.); limu910308@163.com (M.L.); lumin19770919@163.com (M.L.)

* Correspondence: guanxh@neepu.edu.cn; Tel.: +86-1370-440-3650

Received: 27 September 2019; Accepted: 22 October 2019; Published: 25 October 2019

Abstract: A new carbon-coated nickel sulfides electrode material (NST/CNTs@C) has been synthesized through an easy-to-operate process: NiS_2/CNTs which was prepared by a hydrothermal method reacted with BTC (1,3,5-benzenetricarboxylic acid) under the condition of water bath heating to obtain the precursor, and then the precursor was calcined in 450 °C under a nitrogen atmosphere to obtain NST/CNTs@C. The electrochemical performance of NST/CNTs@C has been greatly improved because the formation of a carbon-coated layer effectively increased the specific surface area, reduced the charge transport resistance and inhibited the morphological change of nickel sulfides in the charge–discharge process. Compared with pure NiS_2 and NiS_2/CNTs, NST/CNTs@C presented great specific capacitance (620 $F{\cdot}g^{-1}$ at a current density of 1 $A{\cdot}g^{-1}$), better cycle stability (49.19% capacitance retention after 1000 cycles) and more superior rate capability (when the current density was raised to 10 $A{\cdot}g^{-1}$ the specific capacitance remained 275 $F{\cdot}g^{-1}$).

Keywords: nickel sulfides; carbon nanotubes; carbon-coated; supercapacitors; electrode material

1. Introduction

Nowadays, with the problems of global warming, fossil energy shortage and environmental pollution, developing and improving the utilization rate of renewable energy has become a research hotspot [1]. Therefore, it is necessary to enhance the storage capacity of existing energy storage devices. Supercapacitors (SCs), as some of the most promising energy storage devices, have received extensive attention, due to their high power and energy density [2], long cycle life [3] and being environmentally friendly [4]. SCs has already been widely utilized in many fields including consumer electronics [5], vehicles [6] and wearable devices [7]. As is well-known, the electrode materials are the most significant parts of supercapacitors to achieve charge storage [8]. On the basis of the energy storage mechanism of electrode materials, SCs can be classified as two types: (1) electrical double-layer capacitors (EDLCs) with carbon materials as the electrode materials; (2) pseudocapacitors (PCs) with transition metal compounds and conducting polymers as the electrode materials [9]. Normally, transition metal compounds have higher specific capacitance and energy density than carbon materials and conducting polymers because they not only store energy like carbon materials using double-layer but also occur fast and reversible Faradaic redox reaction [10,11].

In recent years, various transition metal compounds, such as NiO [12], MnO_2 [13], $Ni(OH)_2$ [14], $Co(OH)_2$ [15], CuS [16], NiS [17], and NiS_2 [18], have been studied as electrode materials for supercapacitors. Particularly, nickel sulfides (NiS, NiS_2 and Ni_3S_2 et al.) which are easy to synthesize [19] with multiple valences [20] and low cost [21] have great application potential in supercapacitors. However, nickel sulfides also have some disadvantages, such as low rate capability

and poor cyclability [22–24]. Lu etc. prepared NiS_2 hollow spheres with specific capacitance up to 1643 $F{\cdot}g^{-1}$, but after 1000 cycles, the specific capacitance retention rate was only 27.7% [25]. Yang and his co-workers reported flower-like β-NiS had a specific capacitance of 857.76 $F{\cdot}g^{-1}$ at a current density of 2 $A{\cdot}g^{-1}$, but the specific capacitance sharp decreased when the current density raised to 5 $A{\cdot}g^{-1}$ [26]. The poor cyclic stability and low rate capability limit the practical application of nickel sulfides.

To solve these problems, various nickel sulfide composites have been constructed by combining them with different carbon materials such as carbon nanotubes (CNTs) [27], graphene [28], carbon-coated layer [29], and carbon fiber paper [30]. These carbon materials are usually mixed with transition metal compounds through different patterns, depending on the synthetic methods and types of materials. CNTs as one kind of electrode material has good chemical stability, low mass density, high conductivity, and large surface area [31,32]. Some previous reports have confirmed that the combination of transition metal compounds and CNTs can indeed improve the specific capacitance [33,34]. Moreover, Carbon-coated method can effectively improve the conductivity and mechanical strength of electrode materials, which is conducive to amelioration of electrochemical stability and rate capability. For example, Li's group constructed V_2O_3 nanoflakes@C composites using activated carbon as carbon source, the rate performance of it was higher than pure V_2O_3 nanoflakes [35]. Shao et al. synthesized NiCoOP@C by hydrothermal process, carbonization and phosphorization treatment. Compared with NiCoOP without carbon-coated, the specific capacitance retention increased from 57% (NiCoOP) to 100% (NiCoOP@C) after 3000 cycles [36]. Guo and his co-workers prepared MnO_2@C composite nanorods choosing glucose as carbon source, not only the cyclic stability of the MnO_2@C composite nanorods has been improved but also the charge-transfer resistance was much lower than that of pure MnO_2 [37]. Common carbon sources include glucose [38], soluble starch [39], and sulfonated polystyrene [40]. In this paper, 1,3,5-benzenetricarboxylic acid (BTC) (Aladdin Industrial Corporation, Los Angeles, CA, USA.), a novel carbon source was adopted. BTC is often used as organic skeleton to prepare MOFs, because it contains plenty of oxygen-containing functional groups which has strong adsorption capacity for metal ions and can coordination with metal ions [41,42]. However, using it as carbon source for carbon-coated reaction has rarely been reported. In order to compare the effect of different carbon-coated materials on electrochemical performance of nickel sulfides. BTC, polyaniline (PANI) and glucose were selected as carbon sources. The carbon-coated reaction processes using PANI and glucose were based on the methods of the previous references [43,44]. It can be seen that the specific capacitance, cyclic stability and rate performance of electrode material which used BTC as carbon source were the highest in Table 1. It indicated that using BTC as carbon source had certain advantages.

Table 1. Comparison of specific capacitance, rate capability and stability of samples with different carbon sources.

Carbon Source	C_m ($F{\cdot}g^{-1}$) (Current Density: 1 $A{\cdot}g^{-1}$)	C_m ($F{\cdot}g^{-1}$) (After 1000 Cycles)	C_m ($F{\cdot}g^{-1}$) (Current Density: 10 $A{\cdot}g^{-1}$)
BTC	620	305	275
PANI	535	12.5	25
Glucose	505	7.5	25

Herein, the purpose of our design was to simultaneously improve the specific capacitance and cycle stability of nickel sulfides. CNTs and carbon-coated materials played different roles; the former was introduced to increase the specific capacitance, and the latter was used to further enhance the stability. Firstly, NiS_2/CNTs was prepared by hydrothermal method. The surface of surface-modified CNTs had a mass of polar groups to adsorb Ni^{2+}, and NiS_2 crystallized and grown on the surface of CNTs. Due to synergistic effect between NiS_2 and CNTs, the specific capacitance of NiS_2/CNTs was greatly enhanced. Next, NST/CNTs@C was prepared by water bath heating method and calcination process. BTC organic molecules adsorbed and deposited on the surface of NiS_2/CNTs and possibly happened coordination reaction with NiS_2 in water bath heating process to obtain the precursor [45], and then the precursor was calcined in inert gases to carbonize. The formation of carbon-coated layer

has successfully improved the rate performance and cycle stability. The synthetic route of NST/CNTs@C was shown in Scheme 1.

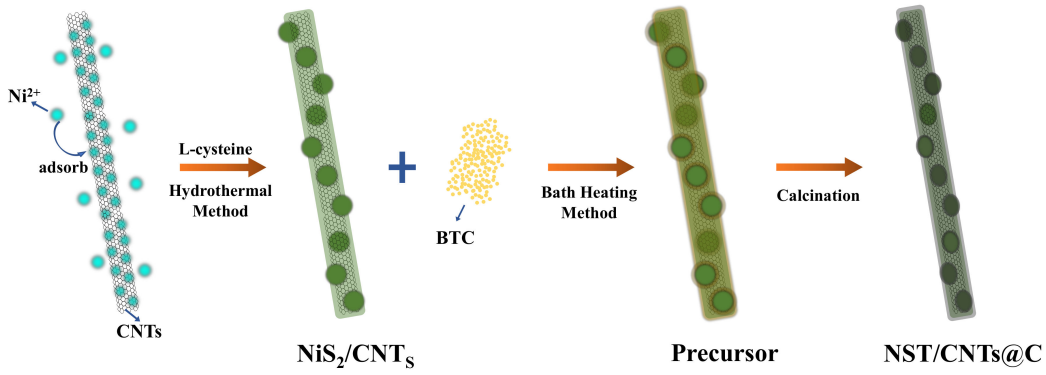

Scheme 1. Schematic illustration of the synthetic route of NST/CNTs@C.

2. Materials and Methods

2.1. Materials

All of the chemical reagents that used in this experiment were analytical grade and without further purification. All of the solutions were formulated with distilled water.

2.2. Surface Modification of CNTs

A sample of 1.0 g raw CNTs (Multi-walled CNTs were purchased from SUSN Limited Company in Shenzhen, China, specific surface area: 85–110 $m^2 \cdot g^{-1}$, diameter: 20–50 nm.) were added into 100 mL of mixture that was constituted by concentrated H_2SO_4 and concentrated HNO_3 (volume ratio of 3:1) with magnetic stirring for 10 min. And then the mixture was heated in water bath at 80 °C for 3 h. After the mixture was cooled to the room temperature, vacuum filter was used to filter the product with water and ethanol until the effluent became neutral. Finally, the product was dried in a vacuum drying oven at 60 °C for 24 h to obtain surface-modified CNTs which were pulverized with the agate mortar and pestle.

2.3. Preparation of NiS_2/CNTs

A sample of 0.2908 g $Ni(NO_3)_2 \cdot 6H_2O$ and 0.0909 g urea were dissolved in 60 mL of distilled water with magnetic stirring for 10 min, and then 0.0123 g surface-modified CNTs were added with ultrasonic treatment for 30 min to disperse evenly, next 0.3635 g L-cysteine was added and ultrasonic treated for 1 h until it was completely dissolved. After that, the solution was transferred into a 100 mL Teflon-lined stainless steel autoclave and subsequently kept at 140 °C for 16 h. After cooling down to the room temperature, the black product was collected and washed with distilled water and ethanol for several times to remove impurity ions by centrifugation. Finally, the product was dried in a vacuum drying oven at 60 °C for 24 h to obtain NiS_2/CNTs. The same method was used to prepare NiS_2 for comparison, just not adding surface-modified CNTs.

2.4. Preparation of NST/CNTs@C

A sample of 0.2456 g NiS_2/CNT_S were added into 40 mL of N, N-Dimethylformamide (DMF) with ultrasonic treatment for 30 min. Meanwhile, 0.1261 g BTC was dissolved into 20 mL of alcohol with ultrasonic treatment for 10 min. After that, these two solutions were mixed together and then the mixture was stirred continuously and heated in water bath at 60 °C for 12 h. After reaction, the black product was collected and washed with DMF and ethanol for several times to remove impurity ions by centrifugation. The product was dried in a vacuum drying oven at 60 °C for 24 h to obtain the

precursor. Finally, the precursor was calcined in 450 °C for 2 h under nitrogen atmosphere at a ramping rate of 1 °C·min^{-1} to obtain NST/CNTs@C.

2.5. Characterization

In order to identify the phase composition and the valence states of samples, powder X-ray diffraction (XRD, XRD-7000, Shimadzu, Chiba, Japan) with a Cu-Kα radiation source and X-ray photoelectron spectroscopy (XPS, ESCALAB-250, Thermo Fisher, Waltham, MA, USA) with an Al-Kα radiation source were used. Scanning electron microscope (SEM, XL-30 FEG, FEI, Hillsborough, OR, USA.) and transmission electron microscope (TEM, TECNAI F20, FEI, Hillsborough, OR, USA) were used to investigate the structure and morphology of the samples. The specific surface area and pore structure were determined by N_2 adsorption/desorption experiment (ASAP 2020 plus HD88, Micromeritics Instrument Corp, Norcross, GA, USA). Chemical bonding information of the studied samples was gathered with Fourier transformed infrared spectroscopy (FTIR, Nicolet iS50, Thermo Fisher Scientific, Waltham, MA, USA).

2.6. Electrochemical Measurements

In this study, Parstat 4000 electrochemical workstation was used to test the electrochemical performance of the samples at room temperature. Three-electrode system including the Hg/HgO electrode as reference electrode, the platinum foil as counter electrode and the working electrode were used. The working electrode was produced by pressing a slurry of active material, acetylene black and polytetrafluoroethylene (mass ratio of 8:1:1) onto the nickel foam (1·1 cm^2), and the load of active material was controlled about 8 mg. 2.0 M KOH solution was adopted as electrolyte solution.

3. Results and Discussion

3.1. Materials Characterization

Surface modification provided abundant oxygenated sites on the surface of CNTs and removed amorphous carbon and impurities [46]. Compared with the raw CNTs, the surface of surface-modified CNTs appeared vibrational peaks of –OH, C=O and C–O et al., (Figure 1a). These polar functional groups can improve the hydrophilicity and adsorption capacity of CNTs. The improvement of hydrophilicity not only enable CNTs to be better dispersed in distilled water but also increase the active sites on CNTs to adsorb Ni^{2+}. As shown in Figure 1b,c, the surface-modified CNTs was more evenly dispersed in distilled water and still wasn't sedimentation after standing 24 h. The diameter of CNTs that almost no changed before and after treatment was approximately 20–50 nm as shown in Figure 1d,e.

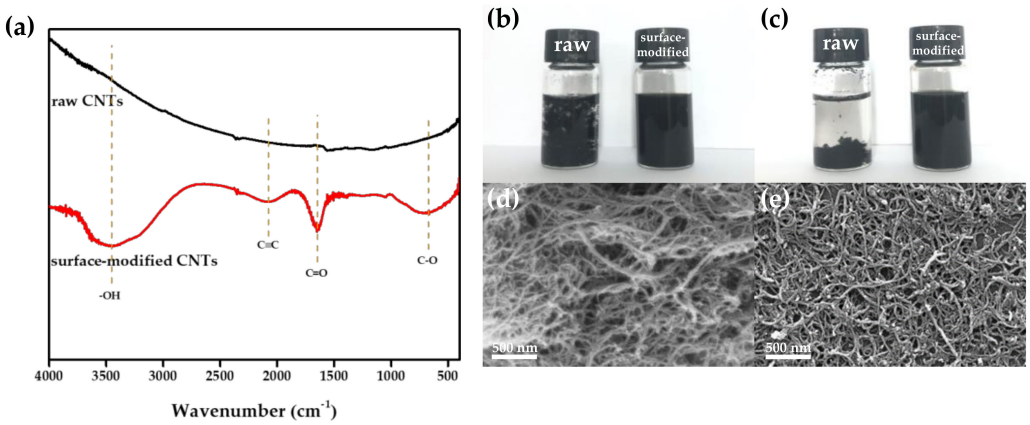

Figure 1. (**a**) FT-IR of the raw CNTs and the surface-modified CNTs; Dispersion state of the raw CNTs and the surface-modified CNTs in distilled water after standing for a certain time: (**b**) 0 h and (**c**) 24 h; (**d**) SEM image of the raw CNTs; (**e**) SEM image of the surface-modified CNTs.

The phase compositions were studied by XRD, the results of NiS_2, NiS_2/CNTs and NST/CNTs@C were shown in Figure 2a. It showed that the peak positions of diffraction peaks of NiS_2 and NiS_2/CNTs were the same, both of which were in accordance with the standard data of cubic NiS_2 (JCPDS No.89–7142). According to references [47,48], the reaction route for the synthesis of NiS_2 could be expressed as the following chemical Equations:

$$HSCH_2CHNH_2COOH + H_2O \rightarrow CH_3COCOOH + NH_3 + H_2S \quad (1)$$

$$H_2NCONH_2 + 3H_2O \rightarrow 2NH_4^+ + 2OH^- + CO_2 \quad (2)$$

$$Ni(NO_3)_2 \rightarrow Ni^{2+} + 2NO_3^- \quad (3)$$

$$Ni^{2+} + 2H_2S + 2OH^- \rightarrow NiS_2 + H_2O + H_2 \quad (4)$$

The diffraction intensity of NiS_2 was stronger than NiS_2/CNTs because the addition of CNTs reduced the crystallinity. NiS_2 happened phase transition during the calcination process, as the result of XRD analysis that NST/CNTs@C include two different phases: one was hexagonal NiS (JCPDS No.77–1624) and the other was cubic Ni_3S_4 (JCPDS No.43–1469). As the XPS spectra of Ni 2p shown in Figure 2b, NiS_2/CNTs exhibited 856.49 eV binding energy which corresponded to the Ni^{2+}. Meanwhile, the Ni^{1+} (853 eV) and Ni^{2+} (855.68 eV) were coexistence in NST/CNTs@C, indicating the characteristic of NiS and Ni_3S_4 [49,50]. Figure 2c revealed that carbon species had been changed, due to carbon-coated layer was formed on the surface of the raw material by carbon-coated treatment [51].

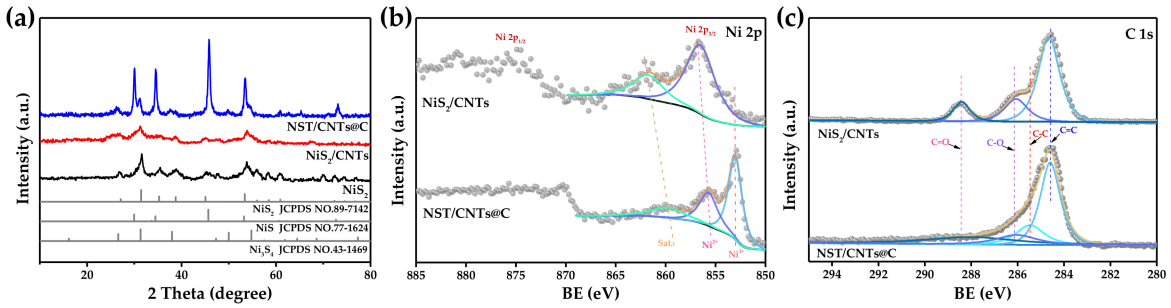

Figure 2. (**a**) X-ray diffraction patterns of three electrode materials; XPS spectra for (**b**) Ni 2p and (**c**) C 1s of NiS_2/CNTs and NST/CNTs@C.

The morphology and microstructure of NiS_2, NiS_2/CNTs and NST/CNTs@C were investigated using SEM and TEM. It can be directly seen that the morphology of NiS_2 was irregular nanoparticles whose surface was rough and diameter was approximately 20–50 nm, as shown in Figure 3a. From Figure 3b,c it can be seen that CNTs were coated with NiS_2 and grown together with NiS_2 nanoparticles. This kind of morphology of NiS_2/CNTs nanocomposites were beneficial to enhance the specific surface area and reaction active sites, which may promote redox reaction and charge transfer [52]. The average diameter of nickel sulfides particles of NST/CNTs@C (Figure 3d) was a little larger than NiS_2/CNTs, and it could obviously be observed that a carbon-coated layer was formed on the surface of NST/CNTs@C in Figure 3e,f. The carbon-coated layer could effectively limit the volume expansion of nickel sulfides in the charge–discharge process [53,54].

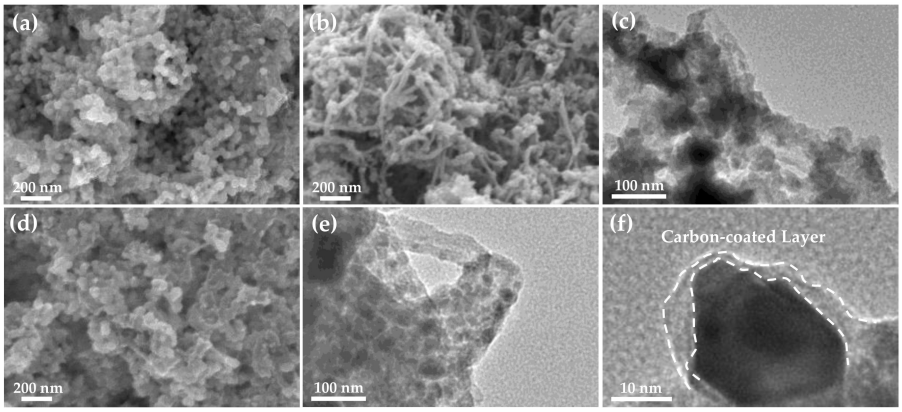

Figure 3. (**a**) SEM image of NiS_2; (**b**) SEM image of NiS_2/CNTs; (**c**) TEM image of NiS_2/CNTs; (**d**) SEM image of NST/CNTs@C; (**e**) TEM image of NST/CNTs@C; (**f**) RHTEM image of NST/CNTs@C.

The specific surface areas and pore structures of NiS_2, NiS_2/CNTs and NST/CNTs@C were investigated using N_2 adsorption/desorption measurement. The adsorption isothermal curves of three electrode materials were type IV adsorption isotherm which were showed in Figure 4a, and the curves revealed distinct hysteresis loops. It indicated that all three materials belong to mesoporous structure. The specific surface areas of NiS_2, NiS_2/CNTs and NST/CNTs@C were 14.39 $m^2 \cdot g^{-1}$, 25.80 $m^2 \cdot g^{-1}$ and 79.51 $m^2 \cdot g^{-1}$, respectively. By compounding with NiS_2, the specific surface area of NiS_2/CNTs had been improved. There were two main reasons: (1) CNTs has a larger specific surface area; (2) The introduction of CNTs improved the dispersity of NiS_2. Moreover, the specific surface area of NST/CNTs@C had been greatly increased. This may be because the carbon-coated layer has larger pore volume (Figure 4b). Furthermore, A large specific surface area provided a higher number of reactive sites for electrode materials to improve the electrochemical properties.

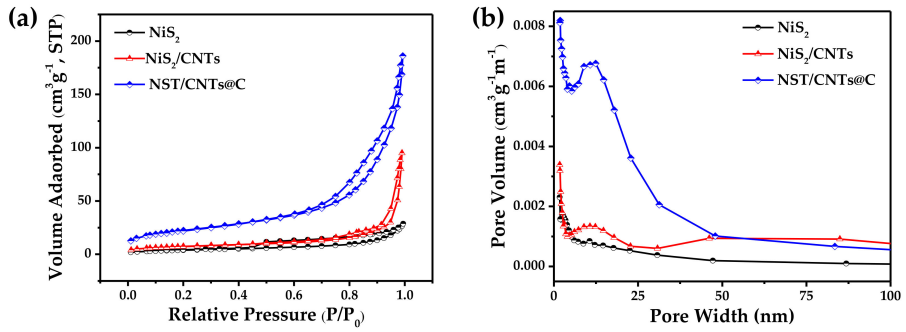

Figure 4. (**a**) N_2 adsorption/desorption isotherms; (**b**) Corresponding pore-size distribution curves.

3.2. Electrochemical Properties

The cyclic voltammetry (CV) curves of NiS_2, NiS_2/CNTs and NST/CNTs@C at a scan rate of 10 $mV \cdot s^{-1}$ within the voltage window from 0 V to 0.5 V are shown in Figure 5a. The CV curves of three electrode materials all had paired redox peaks, which meant all of three kinds of electrode materials that possessed reversible redox reactions and revealed quasi-capacitance ability. Obviously, the CV curve of NiS_2/CNTs presented the largest integrated area corresponded to the maximum specific capacitance. This conclusion was consistent with the consequence of galvanostatic charge–discharge p (GCD) tests shown in Figure 5b. The specific capacitance of NiS_2, NiS_2/CNTs and NST/CNTs@C were calculated according to the Equation (5) to be 430 $F \cdot g^{-1}$, 885 $F \cdot g^{-1}$ and 620 $F \cdot g^{-1}$ at a current density of 1 $A \cdot g^{-1}$, respectively.

$$C_m = (I \cdot \Delta t) / m \Delta V \quad (5)$$

where C_m is the mass specific capacitance (F·g^{-1}), I is the discharge current (A), m is the mass of the active material (g), Δt is the discharge time (s) and ΔV is the voltage range (V), respectively [55]. The specific capacitance has been improved because of the addition of CNTs. Furthermore, the specific capacitance of NST/CNTs@C was lower than NiS_2/CNTs but much higher than NiS_2. It was due to the transformation from NiS_2 into NiS and Ni_3S_4 during the calcination process, and compared with NiS_2 (870 mAh·g^{-1}), NiS (589 mAh·g^{-1}) and Ni_3S_4 (703 mAh·g^{-1}) exhibits an inferior theoretical capacity [56].

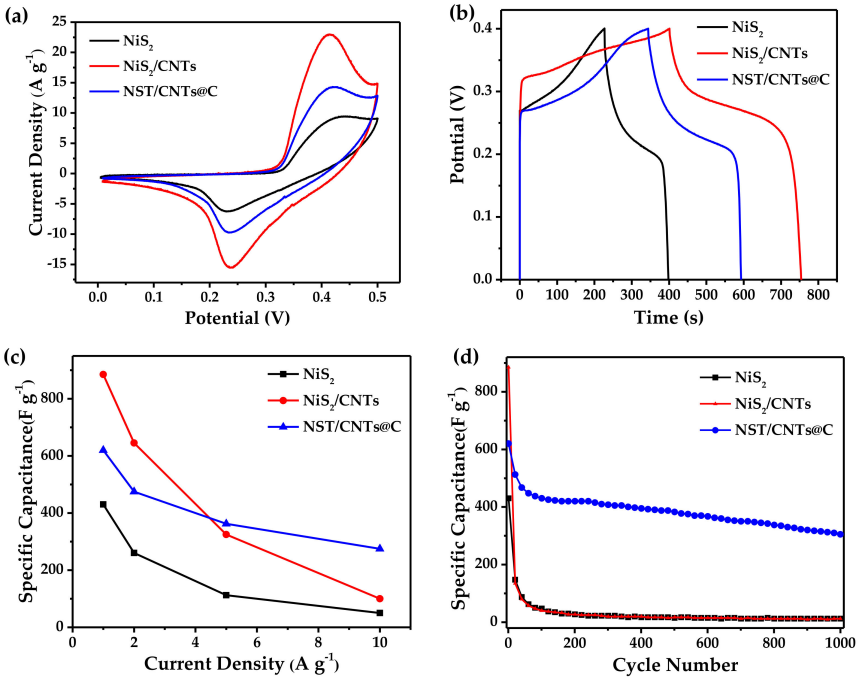

Figure 5. (**a**) CV curves at a scan rate of 10 mV·s^{-1}; (**b**) GCD curves at a current density of 1 A·g^{-1}; (**c**) Specific capacitance at various current density; (**d**) Capacity retention during 1000 cycles of GCDat a current density of 1A·g^{-1}.

As shown in Figure 5c, when the current density was elevated to 5 A·g^{-1}, the specific capacitance of NiS_2, NiS_2/CNTs and NST/CNTs@C declined to 112.5 F·g^{-1}, 325 F·g^{-1} and 362.5 F·g^{-1}, respectively. The specific capacitance of NST/CNTs@C was the highest of the three electrode materials. Moreover, while the current density continued to rise to 10 A·g^{-1}, the specific capacitance retention rates of three kinds of electrode materials were 11.62%, 11.30% and 44.35%, respectively. The above results suggested that although carbon-coated treatment reduced the specific capacitance, it greatly improved the rate performance. Figure 5d shows the cyclic performance of these electrode materials at a current density of 1 A·g^{-1} and the voltage range was from 0 V to 0.4 V. The specific capacitance of NiS_2 and NiS_2/CNTs dropped sharply in the first 20 cycles, from 430 F·g^{-1} and 885 F·g^{-1} declined to 54 F·g^{-1} and 59 F·g^{-1}, respectively. The rapid decrease of specific capacitance may be owing to the transformation of microstructure which was caused by the volume expansion and contraction in the process of redox reactions [57]. After 20 cycles, the morphology of NiS_2 and NiS_2/CNTs electrode materials were presented in Figure 6a,b. The changes of the morphology were enormous, dispersed NiS_2 nanoparticles almost completely disappeared and only the aggregated substances which can't distinguish the original form (Figure 3a,b) can be seen. The introduction of CNTs slightly weakened the degree of morphological damage, but it was hardly helpful to improve stability. However, the specific capacitance of NST/CNTs@C was only reduced from 620 F·g^{-1} to 512.5 F·g^{-1} in the first 20 cycles. That the morphology of NST/CNTs@C maintained almost unchanged after 20 cycles (Figure 6c) suggests that the carbon-coated layer had successfully restrained the volume expansion and contraction in the reaction process. The specific capacitance of all three electrode materials decreased at a relatively slow

rate from the 20th to the 100th cycles and then tended to be stable after 100th cycles. The morphological changes of all three kinds of electrode materials were not obvious from the 20th cycle to the 1000th cycle (Figure 6d–f), which is why the specific capacitance decay rate slowed down. The retention rates of NiS_2, NiS_2/CNTs and NST/CNTs@C were 1.6%, 0.56% and 49.19% after 1000 cycles, respectively. The cycle stability of NST/CNTs@C had been tremendously improved.

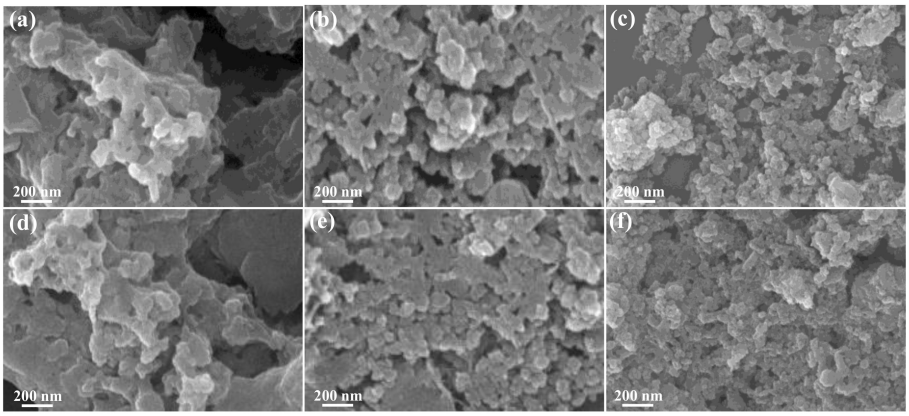

Figure 6. SEM images of (**a**) NiS_2, (**b**) NiS_2/CNTs and (**c**) NST/CNTs@C after 20 cycles; SEM images of (**d**) NiS_2, (**e**) NiS_2/CNTs and (**f**) NST/CNTs@C after 1000 cycles.

The electrochemical performances were further explained by the electrochemical impedance spectroscopy (EIS) text. Figure 7 showed the Nyquist plots which obtained in the frequency range from 100 kHz to 0.01 Hz and the quivalent circuit model of three electrode materials. In general, the Nyquist plot of electrode materials for redox supercapacitors should include a semicircle related to Faradaic reactions in high-frequency region and a straight line related to Warburg impedance in low frequency region [58]. It can be seen from the equivalent circuit model, the electrode systems contained electrolyte solution resistance (R_s), charge transfer resistance (R_{ct}), Warburg impedance resistance in ions diffusion process (Z_w) and the double layer capacitance at the electrode/electrolyte interface (C_{dl}). The R_{ct} of NiS_2, NiS_2/CNTs and NST/CNTs@C can be calculated to be 8.26 Ω, 7.37 Ω and 4.25 Ω, respectively. It clearly revealed that the electronic conductivity had been improved by the introduction of carbon materials. Furthermore, the electronic conductivity may be an influence factor of rate capability. The higher slope of the straight line indicated lower ions diffusion resistance and more outstanding capacitance performance [21]. The sequence of the slopes from low to high: NiS_2, NST/CNTs@C and NiS_2/CNTs. This result was consistent with the CV curves and the GCD curves.

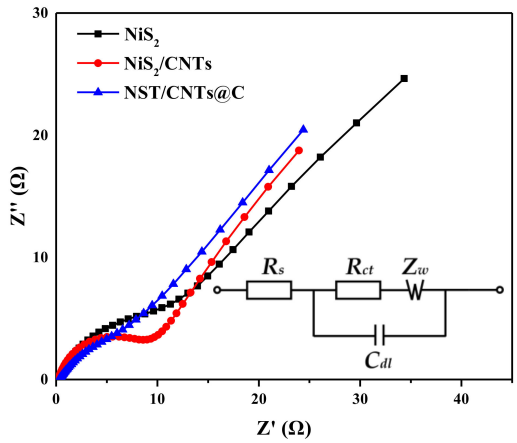

Figure 7. Nyquist plots of NiS_2, NiS_2/CNTs and NST/CNTs@C electrodes, the inset is equivalent circuit model.

4. Conclusions

In summary, we successfully synthesized a new carbon-coated nickel sulfide electrode material (NST/CNTs@C) by introducing two different forms of carbon materials, in which the specific capacitance was increased with the addition of CNTs and the rate performance, and cycle stability were improved by the carbon-coated layer which was formed with BTC as carbon source. The carbon-coated layer effectively enhanced the electrical conductivity and restricted the deformation of nickel sulfides in the process of GCD. Compared with pure NiS_2, the specific capacitance of NiS_2/CNTs raised from 430 $F{\cdot}g^{-1}$ to 885 $F{\cdot}g^{-1}$ at a current density of 1 $A{\cdot}g^{-1}$. And NST/CNTs@C also showed good cycling stablility with 49.19% capacitance retention at 1 $A{\cdot}g^{-1}$ after 1000 cycles (the capacitance retention of NiS_2 and NiS_2/CNTs were only 1.6% and 0.56%). Comprehensively, the introduction of CNTs and carbon-coated layer was an effective method to improve the overall electrochemical properties of nickel sulfides.

Author Contributions: Conceptualization and methodology, X.L. and X.G.; formal analysis, investigation and data curation X.L., M.L. (Min Lu) and M.L. (Mu Li); Writing—Original draft preparation, X.L.; Writing—Review and editing, X.G., X.L., M.L. (Min Lu) and M.L. (Mu Li).

Funding: This project was supported financially by the National Natural Science Foundation of China (no. 51672040), Science and Technology Research Projects of the Education Department of Jilin Province (no. JJKH20180429KJ) and Jilin City Science and Technology Bureau (no. 201750228).

Conflicts of Interest: The authors declare no conflict of interest.

References

1. Wang, J.M.; Liu, Z.; Zheng, Y.W.; Cui, L.; Yang, W.R.; Liu, J.Q. Recent advances in cobalt phosphide based materials for energy-related applications. *J. Mater. Chem. A* **2017**, *5*, 22913–22932. [CrossRef]
2. Zhi, J.; Reiser, O.; Huang, F. Hierarchical MnO_2 spheres decorated by carbon coated cobalt nanobeads: Low cost and high performance electrode materials for supercapacitors. *ACS Appl. Mater. Interfaces* **2016**, *8*, 8452–8475. [CrossRef]
3. Tang, Y.F.; Chen, T.; Yu, S.X.; Qiao, Y.Q.; Mu, S.C.; Zhang, S.H.; Zhao, Y.F.; Hou, L.; Huang, W.W.; Gao, F.M. A highly electronic conductive cobalt nickel sulphide dendrite/quasi-spherical nanocomposite for a supercapacitor electrode with ultrahigh areal specific capacitance. *J. Power Sour.* **2015**, *295*, 314–322. [CrossRef]
4. Ning, T.; Wei, W.; You, H.H.; Zhai, Z.J.; Hilario, J.; Zeng, L.; Liang, Z.; Zhang, L. Morphology tuning of porous CoO nanowall towards enhanced electrochemical performance as supercapacitors electrodes. *Catal. Today* **2018**, *330*, 240–245.
5. Monteiro, J.; Garrido, N.; Fonseca, R. Efficient supercapacitor energy usage in mobile phones. In Proceedings of the 2011 IEEE International Conference on Consumer Electronics-Berlin (ICCE-Berlin), Berlin, Germany, 6–8 September 2011; pp. 318–321.
6. Deka, B.K.; Hazarika, A.; Kim, J.; Park, Y.B.; Park, H.W. Recent development and challenges of multifunctional structural supercapacitors for automotive industries. *Int. J. Energy Res.* **2017**, *41*, 1397–1411. [CrossRef]
7. Sasikala, S.P.; Lee, K.E.; Lim, J.; Lee, H.J.; Koo, S.H.; Kim, I.H.; Jung, H.J.; Kim, S.O. Interface-confined high crystalline growth of semiconducting polymers at graphene fibers for high-performance wearable supercapacitors. *ACS Nano* **2017**, *11*, 9424–9434. [CrossRef] [PubMed]
8. Guan, X.H.; Li, M.; Zhang, H.Z.; Yang, L.; Wang, G.S. Template-assisted synthesis of $NiCoO_2$ nanocages/reduced graphene oxide composites as high-performance electrodes for supercapacitors. *RCS Adv.* **2018**, *8*, 16902–16909. [CrossRef]
9. Kolathodi, M.S.; Palei, M.; Natarajan, T.S. Electrospun NiO nanofibers as cathode materials for high performance asymmetric supercapacitors. *J. Mater. Chem. A* **2015**, *3*, 7513–7522. [CrossRef]
10. Ren, X.C.; Guo, C.L.; Xu, L.Q.; Li, T.T.; Hou, L.F.; Wei, Y.H. Facile synthesis of hierarchical mesoporous honeycomb-like NiO for aqueous asymmetric supercapacitors. *ACS Appl. Mater. Interfaces.* **2015**, *7*, 19930–19940. [CrossRef]
11. Du, W.M.; Zhu, Z.Q.; Wang, Y.B.; Liu, J.N.; Yang, W.J.; Qian, X.F.; Pang, H. One-step synthesis of $CoNi_2S_4$ nanoparticles for supercapacitor electrodes. *RCS Adv.* **2014**, *4*, 6998–7002. [CrossRef]

12. Wu, M.K.; Chen, C.; Zhou, J.J.; Yi, F.Y.; Han, L. MOF—Derived hollow double—Shelled NiO nanospheres for high—Performance supercapacitors. *J. Alloys Compd.* **2018**, *734*, 1–8. [CrossRef]
13. Li, N.; Zhu, C.Z.; Lai, L.Q.; Jiang, R.; Zhu, J.L. Controllable synthesis of different microstructured MnO_2 by a facile hydrothermal method for supercapacitors. *J. Alloys Compd.* **2017**, *692*, 26–33. [CrossRef]
14. Liu, F.Y.; Xiang, C.; Zhang, H.T.; Zhang, B.B.; Su, H.; Jin, L.; Wang, Z.X.; Huang, H.C. Facilely synthesized self-assembly 3D porous $Ni(OH)_2$ with high capacitance for hybrid supercapacitors. *Electrochim. Acta* **2018**, *269*, 102–110. [CrossRef]
15. Cheng, J.P.; Liu, L.; Ma, K.Y.; Wang, X.; Li, Q.Q.; Wu, J.S.; Liu, F. Hybrid nanomaterial of α-$Co(OH)_2$ nanosheets and few-layer graphene as an enhanced electrode material for supercapacitors. *J. Coll. Interface Sci.* **2017**, *486*, 344–350. [CrossRef] [PubMed]
16. Liu, Y.X.; Zhou, Z.X.; Zhang, S.P.; Luo, W.H.; Zhang, G.F. Controllable synthesis of CuS hollow microflowers hierarchical structures for asymmetric supercapacitors. *Appl. Surf. Sci.* **2018**, *442*, 711–719. [CrossRef]
17. Xu, J.L.; Zhang, L.; Xu, G.C.; Sun, Z.P.; Zhang, C.; Ma, X.; Qi, C.L.; Zhang, L.; Jia, D.Z. Facile synthesis of NiS anchored carbon nanofibers for high-performance supercapacitors. *Appl. Surf. Sci.* **2018**, *434*, 112–119. [CrossRef]
18. Akbarzadeh, R.; Dehghani, H. From nickel oxalate dihydrate microcubes to NiS_2 nanocubes for high performance supercapacitors. *J. Solid State Electrochem.* **2018**, *22*, 3375–3382. [CrossRef]
19. Jiang, L.Q.; Qiu, Y.; Lou, P.H.; Yu, Y.L. Nickel hydroxide-impregnated and -coated carbon nanotubes using an easily manipulated solvothermal route for supercapacitors. *Ceram. Int.* **2016**, *42*, 11634–11639. [CrossRef]
20. Pang, H.; Wei, C.Z.; Li, X.X.; Li, G.C.; Ma, Y.H.; Li, S.J.; Chen, J.; Zhang, J.S. Microwave-assisted synthesis of NiS_2 nanostructures for supercapacitors and cocatalytic enhancing photocatalytic H_2 production. *Sci. Rep.* **2014**, *4*, 3577–3589. [CrossRef]
21. Yang, J.Q.; Duan, X.C.; Guo, W.; Li, D.; Zhang, H.L.; Zheng, W.J. Electrochemical performances investigation of NiS/rGO composite as electrode material for supercapacitors. *Nano Energy* **2014**, *5*, 74–81. [CrossRef]
22. Sun, C.H.; Ma, M.Z.; Yang, J.; Zhang, Y.F.; Chen, P.; Huang, W.; Dong, X.C. Phase-controlled synthesis of α-NiS nanoparticles confined in carbon nanorods for high performance supercapacitors. *Sci. Rep.* **2014**, *4*, 7054–7060. [CrossRef] [PubMed]
23. Cai, F.; Sun, R.; Kang, Y.R.; Chen, H.Y.; Chen, M.H.; Li, Q.W. One-step strategy to a three-dimensional NiS deduced graphene oxide hybrid nanostructure for high performance supercapacitors. *RCS Adv.* **2015**, *5*, 23073–23079.
24. Li, X.F.; Shen, J.F.; Li, N.; Ye, M.X. Template-free solvothermal synthesis of NiS_2 microspheres on graphene sheets for high-performance supercapacitors. *Mater. Lett.* **2014**, *139*, 81–85. [CrossRef]
25. Lu, M.; Yuan, X.P.; Guan, X.H.; Wang, G.S. Synthesis of nickel chalcogenide hollow spheres using an L-cysteine-assisted hydrothermal process for efficient supercapacitor electrodes. *J. Mater. Chem. A* **2017**, *5*, 3621–3627. [CrossRef]
26. Yang, J.Q.; Duan, X.C.; Qin, Q.; Zheng, W.J. Solvothermal synthesis of hierarchical flower-like β-NiS with excellent electrochemical performance for supercapacitors. *J. Mater. Chem. A* **2013**, *1*, 7880–7884. [CrossRef]
27. Zhu, T.; Hao, B.W.; Wang, Y.B.; Xu, R.; Lou, X.W. Formation of 1D hierarchical structures composed of Ni_3S_2 nanosheets on CNTs backbone for supercapacitors and photocatalytic H_2 production. *Adv. Energy Mater.* **2012**, *2*, 1497–1502. [CrossRef]
28. Xing, Z.C.; Chu, Q.X.; Ren, X.B.; Tian, J.Q.; Asiri, A.M.; Amary, K.A.; Al-Youbi, A.O.; Sun, X.Q. Biomolecule-assisted synthesis of nickel sulfides/reduced graphene oxide nanocomposites as electrode materials for supercapacitors. *Electrochem. Commun.* **2013**, *32*, 9–13. [CrossRef]
29. Sun, P.; Lin, R.; Wang, Z.; Qiu, M.J.; Chai, Z.S.; Zhang, B.D.; Meng, H.; Tan, S.Z.; Zhao, C.X.; Mai, W.J. Rational design of carbon shell endows TiN@C nanotube based fiber supercapacitors with significantly enhanced mechanical stability and electrochemical performance. *Nano Energy* **2016**, *31*, 432–440. [CrossRef]
30. Cao, L.J.; Tang, G.; Mei, J.; Liu, H. Construct hierarchical electrode with $NixCo_{3-x}S_4$ nanosheet coated on $NiCo_2O_4$ nanowire arrays grown on carbon fiber paper for high-performance asymmetric supercapacitors. *J. Power Sour.* **2017**, *359*, 262–269. [CrossRef]
31. An, K.H.; Kim, W.S.; Park, Y.S.; Moon, J.M.; Bae, D.J.; Lim, S.C.; Lee, Y.S.; Lee, Y.H. Electrochemical properties of high-power supercapacitors using single-walled carbon nanotube electrodes. *Adv. Funct. Mater.* **2001**, *11*, 387–392. [CrossRef]

32. Peigney, A.; Laurent, E.; Flahaut, E.; Bacsa, R.R.; Rousset, A. Specific surface area of carbon nanotubes and bundles of carbon nanotubes. *Carbon* **2001**, *39*, 507–514. [CrossRef]
33. Dubal, D.P.; Holze, R. A successive ionic layer adsorption and reaction (SILAR) method to induce Mn_3O_4 nanospots on CNTs for supercapacitors. *New J. Chem.* **2013**, *37*, 403–408. [CrossRef]
34. Ou, X.; Li, Q.; Xu, D.; Guo, J.G.; Yan, F. In situ growth of MnO_2 nanosheets on *N*-doped carbon nanotubes derived from polypyrrole tubes for supercapacitors. *Chem. Asian J.* **2018**, *13*, 545–551. [CrossRef]
35. Li, H.Y.; Jiao, K.; Wang, L.; Wei, C.; Li, X.L.; Xie, B. Micelle anchored in-situ synthesis of V_2O_3 nanoflakes@C composites for supercapacitors. *J. Mater. Chem. A* **2014**, *2*, 18806–18815. [CrossRef]
36. Shao, Y.B.; Zhao, Y.Q.; Li, H.; Xu, C.J. Three-dimensional hierarchical $NixCo_{1-x}O/Ni_yCo_{2-y}P$@C hybrids on nickel foam for excellent supercapacitors. *ACS Appl. Mater. Interfaces* **2016**, *8*, 35368–35376. [CrossRef] [PubMed]
37. Guo, Z.C.; Mu, J.B.; Che, H.W.; Wang, G.S.; Liu, A.F.; Zhang, X.L.; Zhang, Z.X. Facile preparation of MnO_2@C composite nanorods for high-performance supercapacitors. *J. Mater. Sci.* **2016**, *27*, 13314–13322. [CrossRef]
38. Zheng, H.M.; Zhai, T.; Yu, M.H.; Xie, S.L.; Liang, C.L.; Zhao, W.X.; Wang, S.C.L.; Zhang, Z.S.; Lu, X.H. TiO_2@C core—Shell nanowires for high-performance and flexible solid-state supercapacitors. *J. Mater. Chem. C* **2013**, *1*, 225–229. [CrossRef]
39. Vijayakumar, S.; Nagamuthu, S.; Muralidharan, G. Porous NiO/C nanocomposites as electrode materialfor electrochemical supercapacitors. *ACS Sustain. Chem. Eng.* **2013**, *1*, 1110–1118. [CrossRef]
40. Liang, J.; Xi, K.; Tan, G.Q.; Chen, S.; Zhao, T.; Coxon, P.R.; Kim, H.K.; Ding, S.J.; Yang, Y.; Kumar, R.V.; et al. Sea urchin-like $NiCoO_2$@C nanocomposites for Li-ion batteries and supercapacitors. *Nano Energy* **2016**, *27*, 457–465. [CrossRef]
41. Du, Z.Q.; Li, Y.P.; Wang, X.X.; Wang, J.; Zhai, Q.G. Enhanced electrochemical performance of Li–Co-BTC ternary metal—Organic frameworks as cathode materials for lithium-ion batteries. *Dalton Trans.* **2019**, *48*, 2013–2018. [CrossRef]
42. Salunkhe, R.R.; Kaneit, Y.V.; Yamauchi, Y. Metal-organic framework-derived nanoporous metal oxides toward supercapacitor applications: Progress and prospects. *ACS Nano* **2017**, *11*, 5293–5308. [CrossRef] [PubMed]
43. Sha, C.H.; Lu, B.; Mao, H.Y.; Cheng, J.P.; Pan, X.H.; Lu, J.G.; Ye, Z.Z. 3D ternary nanocomposites of molybdenum disulfide/polyaniline/reduced graphene oxide aerogel for high performance supercapacitors. *Carbon* **2016**, *99*, 26–34. [CrossRef]
44. Xu, K.B.; Zou, R.J.; Li, W.Y.; Liu, Q.; Wang, T.; Yang, J.M.; Chen, Z.G.; Hu, J.Q. Carbon-coated mesoporous NiO nanoparticles as an electrode material for high performance electrochemical capacitors. *New J. Chem.* **2013**, *37*, 4031–4036. [CrossRef]
45. Liu, T.; Liu, Y.X.; Xu, J.; Yao, L.L.; Liu, D.; Wang, C. Conversion of Cu_2O nanowires into Cu_2O/HKUST-1 core/sheath nanostructures and hierarchical HKUST-1 nanotubes. *RSC Adv.* **2016**, *6*, 91440–91444. [CrossRef]
46. Ng, K.C.; Zhang, S.W.; Peng, C.; Chen, G.Z. Individual and bipolarly stacked asymmetrical aqueous supercapacitors of CNTs/SnO_2 and CNTs/MnO_2 nanocomposites. *J. Electrochem. Soc.* **2009**, *156*, A846–A853. [CrossRef]
47. Patil, U.M.; Gurav, K.V.; Fulari, V.J.; Lokhande, C.D.; Joo, O.S. Characterization of honeycomb-like β-$Ni(OH)_2$ thin films synthesized by chemical bath deposition method and their supercapacitor application. *J. Power Sour.* **2009**, *188*, 338–342. [CrossRef]
48. Kun, C.; Chen, W.X. L-cysteine-assisted synthesis of layered MoS_2/graphene composites with excellent electrochemical performances for lithium ion batteries. *ACS Nano* **2011**, *5*, 4720–4728.
49. Wang, J.J.; Zeng, H.C. A hybrid electrocatalyst with a coordinatively unsaturated metal-organic framework shell and hollow Ni_3S_2/NiS core for oxygen evolution reaction applications. *ACS Appl. Mater. Interfaces* **2019**, *11*, 23180–23191. [CrossRef]
50. Cheng, L.L.; Hu, Y.Y.; Ling, L.; Qiao, D.D.; Cui, S.C.; Jiao, Z. One-step controlled synthesis of hierarchical hollow Ni_3S_2/NiS@Ni_3S_4 core/shell submicrospheres for high-performance supercapacitors. *Electrochim. Acta* **2018**, *283*, 664–675. [CrossRef]
51. Shao, Y.; El-Kady, M.F.; Lin, C.W.; Zhu, G.; Marsh, K.L.; Hwang, J.Y.; Zhang, Q.; Li, Y.; Wang, H.; Kaner, R.B. 3D freeze-casting of cellular graphene films for ultrahigh-power-density supercapacitors. *Adv. Mater.* **2016**, *28*, 6719–6726. [CrossRef]

52. Tao, T.; Zhang, L.; Jiang, H.; Li, C.Z. Functional mesoporous carbon-coated CNT network for high-performance supercapacitors. *New J. Chem.* **2013**, *37*, 1294–1297. [CrossRef]
53. Xu, Z.L.; Gang, Y.; Garakani, M.A.; Abouali, S.; Huang, J.Q.; Kim, J.K. Carbon-coated mesoporous silicon microsphere anodes with greatly reduced volume expansion. *J. Mater. Chem. A* **2016**, *4*, 6098–6106. [CrossRef]
54. Du, M.; Rui, K.; Chang, Y.Q.; Zhang, Y.; Ma, Z.Y.; Sun, W.P.; Yan, Q.Y.; Zhu, J.X.; Huang, W. Carbon necklace incorporated electroactive reservoir constructing flexible papers for advanced lithium-ion batteries. *Small* **2018**, *14*, 1702770. [CrossRef] [PubMed]
55. Zheng, C.R.; Cao, C.B.; Ali, Z.; Hou, J. Enhanced electrochemical performance of ball milled CoO for supercapacitor applications. *J. Mater. Chem. A* **2014**, *2*, 16467–16473. [CrossRef]
56. Zhang, Y.R.; Lu, F.; Pan, L.; Xu, Y.; Yang, Y.J.; Bando, Y.; Golberg, D.; Yao, J.N.; Wang, X. Improved cycling stability of NiS_2 cathodes through designing "kiwano" hollow structure. *J. Mater. Chem. A* **2018**, *6*, 11978–11984. [CrossRef]
57. Yuan, Y.F.; Xi, X.H.; Wu, J.B.; Yang, J.L.; Chen, Y.B.; Guo, S.Y. Nickel foam-supported porous $Ni(OH)_2$/NiOOH composite film as advanced pseudocapacitor material. *Electrochim. Acta* **2011**, *56*, 2627–2632. [CrossRef]
58. Li, Y.H.; Xu, J.; Liu, H.; Liu, Y.Y.; Wang, M.R.; Li, J.; Cui, H.T. Surface topography control of NiS/Ni_3S_4 nanosheets for the promotion of electrochemical performance. *J. Sol Gel Sci. Technol.* **2018**, *87*, 546–553. [CrossRef]